# Generation of N00N State With Orbital Angular Momentum in a Twisted Nonlinear Photonic Crystal

Yang Ming, Jie Tang, Zhao-xian Chen, Fei Xu, Li-jian Zhang, and Yan-qing Lu, *Senior Member, IEEE*

*Abstract*—We investigate wavefront engineering of photon pairs generated through spontaneous parametric down conversion in lithium niobate-based nonlinear photonic crystals (NPCs). Due to the complexity of domain structures, it is more convenient to describe photon interaction based on the nonlinear Huygens–Fresnel principle than conventional quasiphase matching regime. Analytical expressions are obtained to describe the transverse properties of down-converted photon states. The convenience of domain engineering in LiNbO$_3$ crystals provides a potential platform for flexible wavefront manipulation of multiphoton states. The generation of N00N state with orbital angular momentum in a twisted NPC is studied utilizing this method. The obtained state is of great value in quantum cryptography, metrology, and lithography applications.

*Index Terms*—N00N state, wavefront engineering, nonlinear photonic crystal, spontaneous parametric down-conversion.

## I. INTRODUCTION

SPONTANEOUS parametric down-conversion (SPDC) is an important approach to obtaining quantum photonic states, such as the heralded single-photon state [1]–[3] and the entangled photon state [4]–[11]. The SPDC process is commonly implemented in $\chi^{(2)}$ nonlinear optical crystals [4], [12], in which a single photon is transformed into a photon pair. In practice, different kinds of complex photon states are required for various specific applications, which need appropriate combinations and modulations of down-converted photons. To perform this task, the so-called nonlinear photonic crystal (NPC) [13] with spatially variable nonlinear coefficient $\chi^{(2)(\vec{r})}$ (the corresponding function is usually periodic or of special form) presents an effective platform. One of the most popular kind of NPC is the domain-inverted ferroelectric crystals which are selectively poled to drive the sign of $\chi^{(2)}$ changing between positive and negative with certain patterns [13], [14]. Among such crystals, the domain-engineered lithium niobate crystal is a valuable candidate [13], [15], [16]. Owing to the mature processing tech-

nologies [17]–[19], suitable domain structure could be flexibly introduced into the LiNbO$_3$ crystals for SPDC engineering [15], [16], [20]. Moreover, the multifunctional feature of LiNbO$_3$ crystal also brings opportunities for function-integrated quantum circuits [11], [15], [21].

In this work, we investigate wavefront engineering of down-converted photons based on domain-engineered LiNbO$_3$ crystals. Tailoring the wavefront of entangled photons has been demonstrated to play an important role in spatial entanglement [20], [22] and orbital angular momentum entanglement of photons [23], which are valuable resources for quantum communication [24], [25], metrology [26], [27] and imaging [16], [28], [29]. In these works, the parametric processes for tailoring wavefront are usually described in conventional phase matching regime. In a NPC, the complexity of domain pattern increases and the corresponding symmetry reduces. It is more convenient to describe the photon interactions based on the nonlinear Huygens–Fresnel principle [30]. Analytical expressions are obtained to outline the wavefront of photon pairs generated from arbitrary domain-engineered LiNbO$_3$ crystals. As an illustration, the SPDC process in a twisted LiNbO$_3$ crystal is investigated. It is revealed that helical wavefront known as orbital angular momentum is imprinted on the N00N state [31].

## II. TRANSVERSE PROPERTIES OF SPDC IN DOMAIN-ENGINEERED LITHIUM NIOBATE CRYSTALS

As is known, inverted domains are introduced into a LiNbO$_3$ crystal through poling it along the direction of optical axis (usually marked as $z$-direction) [17]–[19]. It is relatively convenient to obtain various transverse patterns in the $xy$ plane. Thus, for effective tailoring of the wavefront, we choose to launch the pump light along the $z$-direction. In a usual situation, the $\chi^{(2)}$ coefficient in a single LiNbO$_3$ slice is $z$-independent. However, there is still an available way to realizing $z$-directional modulation of $\chi^{(2)}$ through stacking the slices together [32] (High quality LiNbO$_3$ thin films with a thickness of several hundred nanometers are experimentally achievable through the ion slicing technique [33]). Without loss of generality, we consider a 3-D system, in which the $\chi^{(2)}$ coefficient is $x,y,z$-dependent.

According to nonlinear Huygens–Fresnel principle [30], [34], in SPDC process, each point on the wavefront of the pump light could act as a source of secondary down-converting wavelets through interacting with NPC. The transverse properties of the output photon pairs are determined by the pump and the structure

of NPC together. The influence of each secondary photon pair source on the output photon state could be estimated by the corresponding Hamiltonian density as

$$\mathcal{H}_I(\vec{r}) = \frac{1}{2}\hat{P}_{NL}(\vec{r}) \cdot \hat{E}_p(\vec{r})$$

$$= \frac{1}{2}\chi^{(2)}(\vec{r})\hat{E}_p^{(+)}(\vec{r})\hat{E}_s^{(-)}(\vec{r})\hat{E}_i^{(-)}(\vec{r}), \quad (1)$$

where the subscripts $p$, $s$ and $i$ correspond to the pump, signal and idler photons, respectively. The pump field $E_p$ is usually treated as a classical field and assumed to be undepleted. The signal and idler fields should be quantized and represented by field operators. Detailed expressions are given as follows:

$$E_p^{(+)} = E_{p0}\Psi_{pt}(\vec{r})e^{i(\vec{k}_p \cdot \vec{r} - \omega_p t)}$$

$$E_s^{(-)} = i\sum_{\sigma}\sum_{l_s}\int d\omega_s \int d\vec{k}_s C_{s\sigma} a_{s\sigma}^\dagger e^{-i(\vec{k}_s \cdot \vec{r} + l_s\theta - \omega_s t)}$$

$$E_i^{(-)} = i\sum_{\sigma}\sum_{l_i}\int d\omega_i \int d\vec{k}_i C_{i\sigma} a_{i\sigma}^\dagger e^{-i(\vec{k}_i \cdot \vec{r} + l_i\theta - \omega_i t)}, \quad (2)$$

where $E_{p0}$ is the amplitude of pump light, and $\Psi_{pt}(\tilde{r})$ represents the transverse shape of the field which includes the wavefront information of the pump. Here we consider the monochromatic pump. The parameter $\sigma$ corresponds to the polarization state of the down-converted photons, while $C_{j\sigma}$ ($j = s, i$) is the normalization parameter. The symbols $l_s$ and $l_i$ are defined as topological charge, which indicates that the orbital angular momentum of signal and idler photons are $l_s\hbar$ and $l_i\hbar$, respectively [23]. Moreover, $\theta = tan^{-1}(y/x)$ is the azimuthal coordinate. Based on these analyses, the contribution of a secondary source in the down-converted photon state could be presented through the evolution equation as

$$|d\Psi\rangle = \left[1 - \frac{i}{\hbar}\int_{-\infty}^{\infty}dt\mathcal{H}_I(t)\right]|0\rangle$$

$$= |0\rangle + \frac{iE_{p0}}{2\hbar}\sum_{\sigma,\sigma'}\int d\vec{k}_s \int d\vec{k}_i \int_{-\infty}^{\infty}dtC_{s\sigma}C_{i\sigma'}$$

$$\times K(\vec{r}; \vec{k}_s, \vec{k}_i)e^{-i(\omega_p - \omega_s(\vec{k}_s) - \omega_i(\vec{k}_i))t}a_{s\sigma}^\dagger a_{i\sigma'}^\dagger|0\rangle, \quad (3)$$

with

$$K(\vec{r}; \vec{k}_s, \vec{k}_i) = \chi^{(2)}(\vec{r})\Psi_{pt}(\vec{r})e^{i(\vec{k}_p - \vec{k}_s - \vec{k}_i) \cdot \vec{r}}e^{-i(l_s + l_i)\theta}. \quad (4)$$

The transverse properties of the generated two-photon state are connected to the pump light and the NPC through the function $K(r; k_s, k_i)$. Thus the transverse wavefront of the down-converted photons are determined by the integral of function $K$ in the entire quadratic interaction region. The expression could be given as

$$|\Psi\rangle_f = \int d\vec{r}|d\Psi\rangle$$

$$= |0\rangle + \frac{iE_{p0}}{2\hbar}\sum_{\sigma,\sigma'}\int d\vec{k}_s \int d\vec{k}_i C_{s\sigma}C_{i\sigma'}$$

$$\times \Omega(\vec{k}_s, \vec{k}_i)a_{s\sigma}^\dagger a_{i\sigma'}^\dagger|0\rangle, \quad (5)$$

with

$$\Omega(\vec{k}_s, \vec{k}_i) = \int d\vec{r}K(\vec{r}; \vec{k}_s, \vec{k}_i)\delta(\omega_p - \omega_s(\vec{k}_s) - \omega_i(\vec{k}_i)). \quad (6)$$

where the Dirac-$\delta$ function is given by the temporal integration. The final state is formed through superposing the contributions of all secondary down-converting sources. The spatial integral $\Omega(k_s, k_i)$ represents the correspondence between nonlinear Huygens–Fresnel principle and the superposition principle of quantum states.

Wavefront engineering could be realized through appropriate design of the spatial distribution of the nonlinear coefficient $\chi^{(2)}$, which could be expressed as

$$\chi^{(2)}(\vec{r}) = \chi_{\text{eff}}^{(2)}\sum_{Z_n}G(z|Z_n)\,\text{sgn}\{\cos[2\pi F_{Z_n}(\vec{r}_t)]\}. \quad (7)$$

In the equation, the function $G(z|Z_n)$ represents the $z$-dependence of $\chi^{(2)}$. As is mentioned above, to date $z$-directional modulation of $\chi^{(2)}$ could only be achieved through stacking $LiNbO_3$ slices together, so it is treated discretely. $F_{Zn}(\vec{r}_t)$ corresponds to the transverse domain pattern of the nth $LiNbO_3$ slice. Complex transverse domain structures can be produced conveniently with current techniques. In theory, $F_{Zn}(\vec{r}_t)$ could be arbitrary 1D or 2D function. Reasonable combinations of the functions $G(z|Z_n)$ and $F_{Zn}(\vec{r}_t)$ are critical for elaborate wavefront engineering.

## III. N00N STATE WITH ORBITAL ANGULAR MOMENTUM

In this section, utilizing the approach discussed above, we investigate wavefront engineering of the well-known N00N state in twisted NPCs. A N00N state is expressed as

$$|N :: 0\rangle = (|N, 0\rangle + |0, N\rangle)/\sqrt{2}, \quad (8)$$

where $N$ is a positive integer which represents the number of photons. Such states are very useful in quantum precise phase measurement [35] and super-resolution quantum lithography [36]. The actual effect of N00N state in these applications increases with the photon number $N$. As we know, the two-photon N00N state could be easily experimentally generated through various methods [31], [37]–[40]. However, multi-photon N00N state ($N > 2$) is hard to produce because of technical difficulties [41]. In the following text, we will show that a two-photon N00N state carrying orbital angular momentum may work like a multi-photon N00N state in certain applications. Through appropriate wavefront engineering based on a NPC with a twisted domain pattern, helical wavefront could be imprinted on the photons of a N00N state with $N = 2$. As is known, the helical wavefront corresponds to the orbital angular momentum of a photon [23].

For the transverse domain structure of the NPC, we choose the "Fork Grating" (FG) pattern. In classical linear optics, such patterns are widely used to generate optical vortex with helical wavefront expressed as $\Psi = \exp(im\theta)$ [42]. The illustrations of FGs are given in Fig. 1(a) and (b). Second harmonic generation in this kind of NPC with FG has also been well investigated [14], [43]. Besides, the interaction of transverse structured light and nonlinear optical crystals is also a recent research hotspot [44].
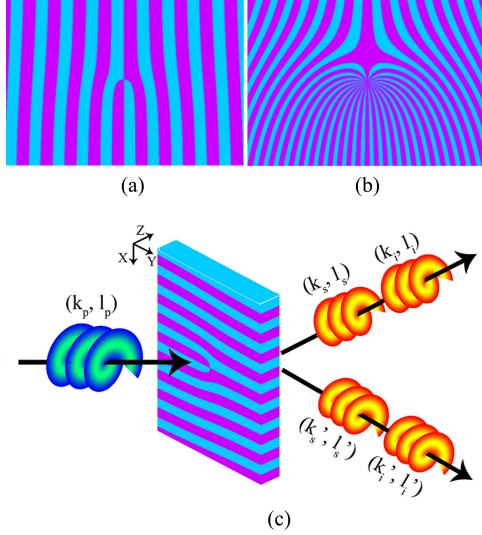
Fig. 1. The FG patterns are plotted based on different topological charges as (a) $l_C = 1$ and (b) $l_C = 20$, which also correspond to transverse domain structures of the LiNbO$_3$-based NPCs. The light blue and purple regions are positive and negative domains, respectively. (c) Schematic of wavefront engineering of N00N state in a twisted NPC. Please note that the helical wavefront does not correspond to the actual value of topological charge, which is just a diagram.

In this work, we would focus on the properties of the quantum state generated in such twisted NPC through SPDC process. The nonlinear coefficient $\chi^{(2)}$ could be written as

$$\chi^{(2)}(\vec{r}) = \chi^{(2)}_{\text{eff}} G[\text{Int}(z/a)]\text{sign}\{\cos[2\pi F(\vec{r}_t) + l_C \theta]\}, \quad (9)$$

where Int(x) refers to the floor function and $a$ is the thickness of a LiNbO$_3$ slice. The function $G[\text{Int}(z/a)]$ is used to distinguish which LiNbO$_3$ slice a $z$-coordinate is located in and describe the influence of the corresponding slice on $\chi^{(2)}$. The value $l_C$ relates to the number of branchings in the central "fork" of the pattern, while $\theta$ is the azimuthal coordinate. $N_{LN}$ is the total number of LiNbO$_3$ slices.

The pump light is set to be $E_p(\vec{r}) = E_{p0}\exp(ik_{pz}z + il_p\theta)$ with the topological charge marked as $l_p$, thus the function $\Psi_{pt}(\vec{r})$ is corresponding to $\exp(il_p\theta)$. Substituting $\Psi_{pt}(\vec{r})$ and Eq. (9) into Eq. (6), we have

$$\Omega_I = \chi^{(2)}_{\text{eff}}\left( \int dz G[\text{Int}(z/a)]e^{i(k_{pz}-k_{sz}-k_{iz})z} \right)$$

$$\times \int d\vec{r}_t\text{sign}\{\cos[2\pi F(\vec{r}_t) + l_C \theta]\}e^{i(l_p - l_s - l_i)\theta}e^{-i(\vec{k}_{st}+\vec{k}_{it})\cdot\vec{r}_t}. \quad (10)$$

In the transverse integral, the function $F(\vec{r}_t)$ is a 1-D or 2-D function. For the FG pattern, we have $F(\vec{r}_t) = x/\Lambda$. $\Lambda$ is defined as the poling period in the $x$-direction. To obtain a clear physical description, the sign function is analyzed with Fourier transform. The set of Fourier basis is chosen to be $\{\exp[im(2\pi x/\Lambda + l_C\theta)]\}$. The expression of is $\chi^{(2)} = \chi_{\text{eff}}\Sigma_m F_m \exp(i2\pi mx/\Lambda)\exp(iml_C\theta)$, where $F_m$ is the Fourier coefficient calculated by $F_m = (1/2\pi) \int \text{sign}[\cos(2\pi x/\Lambda + l_C\theta)] \cdot \exp[im(2\pi x/\Lambda + l_C\theta)]$. In

all the oscillating terms, the first-order terms with $m = \pm 1$ are dominant[14]. Neglecting high-order terms, the transverse integral could be written as

$$I_t = \sum_{\pm 1} F_{\pm 1} \int d\vec{r}_t e^{i(l_p \pm l_C - l_s - l_i)\theta} e^{\pm i\frac{2\pi x}{\Lambda}} e^{-i(\vec{k}_{st}+\vec{k}_{it})\cdot\vec{r}_t}. \quad (11)$$

For the $z$-directional dependence of $\chi^{(2)}$, we would consider a simple case in which the transverse patterns of all LiNbO$_3$ slices are the same but they are placed parallelly and anti-parallelly to the $z$-axis in turn. That means the function $G[\text{Int}(z/a)]$ is expressed as

$$G[\text{Int}(z/a)] = (-1)^{\text{Int}(z/a)}. \quad (12)$$

Based on the analyses above, the state vector of SPDC could be obtained through substituting Eqs. (10)–(12) into Eq. (5), which is expressed as

$$|\Psi\rangle_f = |0\rangle + \sum_{\pm 1} \frac{iE_{p0}F'_{\pm 1}d_{22}}{2\hbar} \int d\vec{k}_s \int d\vec{k}_i C_{s\sigma} C_{i\sigma'}$$

$$\times \left[ \int_0^{N_{LN} a} dz(-1)^{\text{Int}(z/a)} e^{i(k_{pz}-k_{sz}-k_{iz})z} \right]$$

$$\times \left[ \int d\vec{r}_t e^{\pm i\frac{2\pi x}{\Lambda}} e^{-i(\vec{k}_{st}+\vec{k}_{it})\cdot\vec{r}_t} e^{i(l_p \pm l_C - l_s - l_i)\theta} \right] a^\dagger_{s\sigma} a^\dagger_{i\sigma'} |0\rangle. \quad (13)$$

In the equation, only the influence of the first order terms of $\chi^{(2)}$ are included. On the one hand, the transformation efficiencies of the high-order terms are relatively low; on the other hand, as the output angles of down-converted photons are different, their contributions could be eliminated through proper post-selections. The pump light is incident along $z$-direction and assumed to be $y$-polarized. In this situation, the only available element in nonlinear coefficient of LiNbO$_3$ is $d_{22}$, and the down-converted photons should also be $y$-polarized. In the practical diffraction process, the polarization state of photon may be influenced by non-idealities, and the $d_{31}$-dominated nonlinear process may contribute to the down-converted photons. However, this proportion of the contribution is quite small and does not have crucial influences on the final conclusion, thus we neglect that in calculations for simplicity. In practical situations, it is also convenient to eliminate the corresponding influence through putting additional polarizers after the LiNbO$_3$ crystal into the optical paths. Based on these analyses, the summation about the polarization state could be simplified. The characteristics of the down-converted state are derived from Eq. (13). In a high efficiency situation, the obtained photons are imprinted with helical wavefront $\exp[i(l_p \pm l_C)\theta]$ corresponding to a total angular momentum $(l_p \pm l_C)\hbar$.

For the integral term $\int d\vec{r}_t \exp(\pm i2\pi x/\Lambda) \times \exp[-i(\vec{k}_{st} + \vec{k}_{it}) \cdot \vec{r}_t]$, the generation efficiencies of corresponding spatial modes are determined by its modular square. The modular square is calculated to be proportional to $\text{sinc}^2[(k_{sx} + k_{ix} \pm 2\pi/\Lambda)X_0/2] \cdot \text{sinc}^2[(k_{sy} + k_{iy})Y_0/2]$, where $X_0$ and $Y_0$ represent the transverse sizes of the NPC. Just as what is utilized in Ref. [4], two desired modes could be selected with equally

high transformation efficiencies, in which we have $k_{sx} = k_{ix} = \pm\pi/\Lambda$ and $k_{sy} = k_{iy} = 0$ together with a degenerate frequency of the signal and idler photons. This corresponds to two equal possibilities. In both cases, a pair of photons is emitted from the NPC with an angle of equal degree but opposite direction, as is shown in Fig. 1(c). Thus a N00N state is formed. Unlike conventional N00N states [37]–[41], this N00N state possesses optical angular momentum. In practical applications, band pass filters with certain center frequency could be place at the corresponding angles to improve the purity of the state.

The $z$-directional integral $\int_0^{N_{LN}a} dz(-1)^{\mathrm{Int}(z/a)}$ $e^{i(k_{pz}-k_{sz}-k_{iz})z}$ also has critical influences on the transformation efficiency of SPDC process. To improve the transformation efficiency, the value of $a$ should be set at the coherent length decided by $L_{coh} = 2/(k_{pz} - k_{sz} - k_{iz})$. This point could also be understood through the QPM regime. When $N_{LN}$ becomes a large number, it is also convenient to express the function as $\mathrm{sgn}[\sin(2\pi z/L_{coh})]$. Under this condition, the transformation efficiency increases with $N_{LN}$. For a detailed understanding, we calculate the values of transformation efficiency for a practical system with $N_{LN} = 1, 10, 50$, respectively. The pump wavelength is set at 0.405 $\mu$m, while the corresponding signal and idler wavelengths are 0.81 $\mu$m. The coherent length is calculated to be 1.07 $\mu$m. The values of $l_p$ and $l_C$ are assumed to be 3 and 1. The poling period in the $x$-direction is 10.3 $\mu$m, which is determined by $\Lambda = 0.405/n_{PDC} \cdot \sin\theta_{PDC} (\mu\mathrm{m})$ with the propagation angles of down-converted photons $\theta_{PDC} = \pm 1°$. The output angle after exiting NPC will be $\theta_{\mathrm{out}} \sim n_{PDC} \cdot \theta_{PDC} = \pm 2.25°$. When the pump power 1 W, the transformation efficiencies are $1.227 \times 10^{-19}, 4.973 \times 10^{-17}, 6.216 \times 10^{-15}$, respectively. These values are obtained through the coupled wave equations for quadratic nonlinear interaction[14]. The average generation rates of N00N state are calculated to be 0.25, 101.28 and 12659.88 $\mathrm{s}^{-1}$, respectively.

To present quantum interference, the N00N state with orbital angular momentum could be adjusted and detected through the combinations of several optical components, such as Dove prism [45], [46], $q$-plate [47] and the HOM interferometer [31]. The function of a Dove prism is rotating the wavefront [45], [46]. The scheme is shown in Fig. 2(a). Since the down-converted photons pass through the Dove prisms in different arms, the corresponding photonic state could be expressed as

$$|\Psi\rangle \propto \sum_{l_s,l_s'} \left( e^{i(l_s+l_i)\alpha} \left|1_{l_s}+1_{l_i},0_{l_s',l_i'}\right\rangle \right.$$

$$\left. + e^{i(l_s'+l_i')\alpha} \left|0_{l_s,l_i},1_{l_s'}+1_{l_i'}\right\rangle \right)$$

$$\propto \sum_{l_s,l_s'} \left( e^{i(l_p+l_C)\alpha} \left|1_{l_s}+1_{l_i},0_{l_s',l_i'}\right\rangle \right.$$

$$\left. + e^{i(l_p-l_C)\alpha} \left|0_{l_s,l_i},1_{l_s'}+1_{l_i'}\right\rangle \right)$$

$$\propto \sum_{l_s,l_s'} \left( \left|1_{l_s}+1_{l_i},0_{l_s',l_i'}\right\rangle + e^{-i2l_C\alpha} \left|0_{l_s,l_i},1_{l_s'}+1_{l_i'}\right\rangle \right)$$
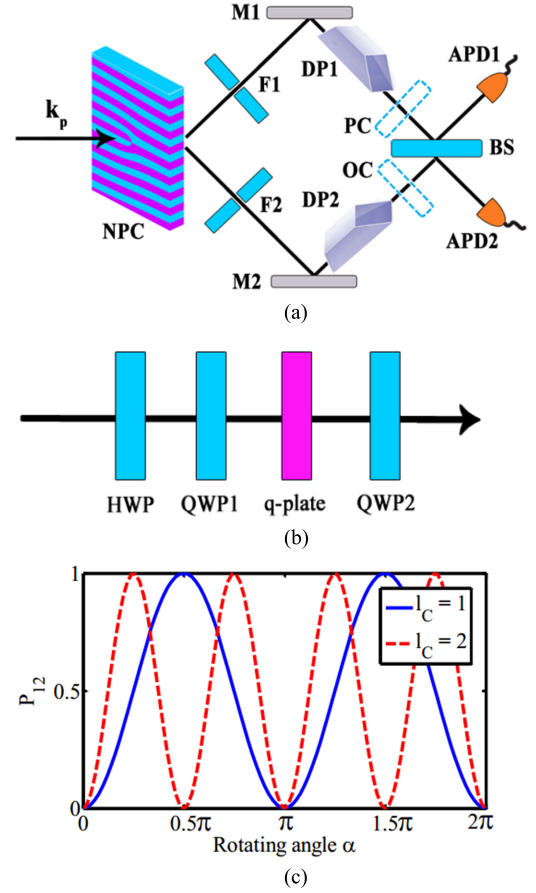
$$\tag{14}$$



Fig. 2. (a) The scheme of quantum coherence based on the N00N state with orbital angular momentum. The meanings of the corresponding symbols are listed as follows, F1 & F2: band-pass filters, M1 & M2: mirrors, DP1 & DP2: Dove prisms, BS: beam splitter, APD1 & APD2: avalanche photodiodes, OC (for $l_p \neq 0$): orbital angular momentum converter, PC (for $l_p \neq 0$): phase compensator. (b) The detailed construction of OC. HWP: half wave plate, QWP: quarter wave plate. (c) The probability of two-photon coincidence against the rotating angle $\alpha$ corresponding to a two-photon N00N state with $l_C = 1$ and $l_C = 2$.

where $\alpha$ is the rotating angle of Dove prism. In this equation, the orbital angular momentums of the generated photons are marked as $(l_s, l_i)$ and $(l_s', l_i')$. The four parameters are topological charges of corresponding photons. After they output from the NPC, we have $l_s + l_i = l_p + l_C$ and $l_s' + l_i' = l_p - l_C$. The two-photon coincidence could be measured utilizing a HOM interferometer. It is worth mentioning that the azimuthal index $l$ of a reflective photon becomes $-l$. The coincidence rate when APD1 detects a photon with OAM $l_1\hbar$ and APD2 detects a photon with OAM $l_2\hbar$ is expressed as

$$R_C \propto \langle\Psi_f| b_{l_1}^\dagger b_{l_2}^\dagger b_{l_2} b_{l_1} |\Psi_f\rangle. \tag{15}$$

In this equation, the subscript 1 and 2 correspond to the upper and lower paths after the beam splitter, respectively. The values of $l_1$ and $l_2$ are chosen from those of $l_s, -l_s', l_i$, and $-l_i'$. The vector $|\psi_f\rangle$ corresponds to the state after the beam splitter. For any given value of $l_p$ and $l_C$, the perfect two-photon coincidence appears only when the orbital angular momentum of down-converted photons satisfies that $l_s + l_i = -l_s' - l_i'$ and either $l_s = -l_s'$ & $l_i = -l_i'$ or $l_s = -l_i'$ & $l_i = -l_s'$. In this case, the terms $|1_{l_1}, 1_{l_2}\rangle$ and $|1_{l_1'}, 1_{l_2'}\rangle$ are indistinguish-

able for maximal interference, and it is convenient to calculate the corresponding probability of coincidence for each possible combination of $l_s$, $l_i$, $l_s{}'$ and $l_i{}'$. In practical measurement, appropriate post-selections of OAM may be done according to the values of $l_s$, $l_i$, $l_s{}'$ and $l_i{}'$ to ensure maximal interference before detection. The approach is similar to that in Ref. [23]. For the other cases when the mentioned condition is not satisfied, the corresponding two terms are independent and there is no interference. Based on these analyses, detailed treatments could be divided into two cases:

i) $l_p = 0$, the condition of maximal interference is automatically satisfied. The probability of two-photon coincidence is

$$P_{12} = \frac{1}{2}[1 - \cos(2l_C\alpha)]. \tag{16}$$

ii) $l_p \neq 0$, the total orbital angular momentum of down-converted photons on the two paths is equal to $(l_p + l_C)\hbar$ and $(l_p - l_C)\hbar$, respectively. To achieve the maximal condition, an additional orbital angular momentum converter (OC) has to be used. We choose the well-known $q$-plate [47]. The typical design of OC is shown in Fig. 2(b). The half wave plate (HWP) and quarter wave plate (QWP) before the $q$-plate are utilized to transform the linearly polarized photons into right-handed circularly polarized photons. The $q$ value is set at $l_p/2$. After passing through the $q$-plate, each photon obtains a part of extra orbital angular momentum of $-l_p\hbar$ and further becomes a left-handed circularly polarized photon. The total orbital angular momentum of the down-converted photons thus is changed into $[(l_s{}'-l_p) + (l_i{}'-l_p)]\hbar = [(l_p - l_C) - 2l_p]\hbar = (-l_C - l_p)\hbar$. The QWP2 after the $q$-plate makes the photons linearly polarized along $y$-direction again. Moreover, a phase compensator (PC) should be placed in the upper path to balance the phase shift caused by the OC. The probability of coincidence also has the same expression as Eq. (16).

In Fig. 2(c), the two-photon coincidence probability is plotted against the rotating angle $\alpha$. It is worth mentioning that the Dove prism influences the polarization state of photon. However, as is shown in Refs. [45], [46], the influence is quite low at short wavelength band. The effect of coherence is nearly unaffected.

In practical applications of N00N state, the photon number is preferred to be large. The precision of phase measurement and the resolution of quantum lithography are both proportional to *1/N* [35], [36]. However, increasing the photon number of N00N state brings great technical challenges in photonic state manipulation and detection. On the contrary, the measurement of angular displacement can be greatly benefited from our two-photon N00N state with orbital angular momentum, which is expressed as $(|2, 0\rangle + e^{i2l_C\alpha} |0, 2\rangle)/\sqrt{2}$, and the related limit of angular resolution is *1/2l_C*. With this state, increasing the photon number of N00N state can be avoided, while the estimation precision can be improved through increasing the value of $l_C$. It has been shown that OAM of light can be used to detect the structure and motion of rotating objects. Thus the quantum

enhancement provided by the N00N state with OAM may find wide applications in remote sensing [48]–[50].

## IV. CONCLUSION

In summary, we investigate wavefront engineering of photon pairs generated through SPDC in domain-engineered $LiNbO_3$ crystals which is a kind of the well-known NPC. The photon interaction processes in $LiNbO_3$ crystals with complex domain patterns are described based on the nonlinear Huygens–Fresnel principle. Analytical expressions about the wavefront of photon pairs generated from arbitrary domain-engineered $LiNbO_3$ crystals are obtained. As a detailed illustration, the generation of N00N state with orbital angular momentum in a twisted $LiNbO_3$ crystal is presented. Such state can be utilized to increase the information capacity of quantum-secured communications [23] as well as to achieve the quantum-enhanced sensing [26]. Besides the azimuthal index (topological charge), the radial index may further expand the degrees of freedom in the system based on nonlinear optical interaction of Laguerre–Gaussian (LG) modes, which has been realized with lithium-niobate-based NPCs [51]. The flexible domain design in $LiNbO_3$ crystals provides a powerful platform for wavefront engineering of two-photon states, which may present a new sight for function-integrated quantum photonic applications.

## REFERENCES

[1] T. B. Pittman, B. C. Jacobs, and J. D. Franson, "Heralding single photons from pulsed parametric down-conversion," *Opt. Commun.*, vol. 246, pp. 545–550, Feb. 2005.

[2] E. Pomarico, B. Sanguinettil, C. I. Osorio, H. Herrmann, and R. T. Thew, "Engineering integrated pure narrow-band photon sources," *New. J. Phys.*, vol. 14, pp. 033008-1–033008-13, Mar. 2012.

[3] T. Jennewein, M. Barbieri, and A. G. Whiteb, "Single-photon device requirements for operating linear optics quantum computing outside the post-selection basis," *J. Mod. Opt.*, vol. 58, pp. 276–287, Feb. 2011.

[4] P. G. Kwiat, K. Mattle, H. Weinfurter, and A. Zeilinger, "New high-intensity source of polarization-entangled photon pairs," *Phys. Rev. Lett.*, vol. 75, pp. 4337–4341, Dec. 1995.

[5] H. Takesue and K. Inoue, "Generation of polarization-entangled photon pairs and violation of Bell's inequality using spontaneous four-wave mixing in a fiber loop," *Phys. Rev. A*, vol. 70, pp. 031802(R)-1–031802(R)-4, Sep. 2004.

[6] M. Hunault, H. Takeuse, O. Tadanaga, Y. Nishida, and M. Asobe, "Generation of time-bin entangled photon pairs by cascaded second-order nonlinearity in a single periodically poled LiNbO₃ waveguide," *Opt. Lett.*, vol. 35, pp. 1239–1241, Apr. 2010.

[7] R. T. Horn *et al.*, "Inherent polarization entanglement generated from a monolithic semiconductor chip," *Sci. Rep.*, vol. 3, pp. 2314-1–2314-5, Jul. 2013.

[8] R. T. Thew, A. Acin, H. Zbinden, and N. Gisin, "Bell-type test of energy-time entangled qutrits," *Phys. Rev. Lett.*, vol. 93, pp. 010503-1–010503-4, Jul. 2004.

[9] J. L. Smirr *et al.*, "Optimal photon-pair single-mode coupling in narrow-band spontaneous parametric down-conversion with arbitrary pump profile," *J. Opt. Soc. Amer. B*, vol. 30, pp. 288–301, Feb. 2013.

[10] J. F. Dynes *et al.*, "Efficient entanglement distribution over 200 kilometers," *Opt. Exp.*, vol. 17, pp. 11440–11449, Jul. 2009.

[11] Y. Ming *et al.*, "Integrated source of tunable nonmaximally mode-entangled photons in a domain-engineered lithium niobate waveguide," *Appl. Phys. Lett.*, vol. 104, pp. 171110-1–171110-4, Apr. 2014.

[12] M. Fiorentino *et al.*, "Spontaneous parametric down-conversion in periodically poled KTP waveguides and bulk crystals," *Opt. Exp.*, vol. 15, pp. 7479–7488, Jun. 2007.

[13] V. Berger, "Nonlinear photonic crystals," *Phys. Rev. Lett.*, vol. 81, pp. 4136–4139, Nov. 1998.

[14] N. V. Bloch *et al.*, "Twisting light by nonlinear photonic crystals," *Phys. Rev. Lett.*, vol. 108, pp. 233902-1–233902-5, Jun. 2012.

[15] Y. Ming *et al.*, "Tailoring entanglement through domain engineering in a lithium niobate waveguide," *Sci. Rep.*, vol. 4, pp. 4812-1–4812-9, Apr. 2014.

[16] P. Xu and S. N. Zhu, "Review article: Quasi-phase-matching engineering of entangled photons," *AIP Adv.*, vol. 2, pp. 041401-1–041401-11, Dec. 2012.

[17] R. G. Batchko, V. Y. Shur, M. M. Fejer, and R. L. Byer, "Backswitch poling in lithium niobate for high-fidelity domain patterning and efficient blue light generation," *Appl. Phys. Lett.*, vol. 75, pp. 1673–1675, Sep. 1999.

[18] A. C. Busacca, S. Stivala, L. Curcio, and G. Assanto, "Parametric conversion in micrometer and submicrometer structured ferroelectric crystals by surface poling," *Int. J. Opt.*, vol. 2012, pp. 606892-1–606892-11, 2012.

[19] D. Yudistira *et al.*, "UV direct write metal enhanced redox (MER) domain engineering for realization of surface acoustic devices on lithium niobate," *Adv. Mater. Interfaces*, vol. 1, pp. 1400006-1–1400006-7, Jul. 2014.

[20] J. P. Torres, A. Alexandrescu, S. Carrasco, and L. Torner, "Quasi-phase-matching engineering for spatial control of entangled two-photon states," *Opt. Lett.*, vol. 29, pp. 376–378, Feb. 2004.

[21] D. Bonneau *et al.*, "Fast path and polarization manipulation of telecom wavelength single photons in lithium niobate waveguide devices," *Phys. Rev. Lett.*, vol. 108, pp. 053601-1–053601-5, Feb. 2012.

[22] C. H. Monken, P. H. Souto Ribeiro, and S. Padua, "Transfer of angular spectrum and image formation in spontaneous parametric down-conversion," *Phys. Rev. A*, vol. 57, pp. 3123–3126, Apr. 1998.

[23] A. Mair, A. Vaziri, G. Weihs, and A. Zeilinger, "Entanglement of the orbital angular momentum states of photons," *Nature*, vol. 412, pp. 313–316, Jul. 2001.

[24] A. Vaziri, G. Weihs, and A. Zeilinger, "Experimental two-photon, three-dimensional entanglement for quantum communication," *Phys. Rev. Lett.*, vol. 89, pp. 240401-1–240401-4, Dec. 2002.

[25] Y. Sun, Q. Y. Wen, and Z. Yuan, "High-efficient quantum key distribution based on hybrid entanglement," *Opt. Commun.*, vol. 284, pp. 527–530, Jan. 2011.

[26] N. Thomas-Peter *et al.*, "Real-world quantum sensors: Evaluating resources for precision measurement," *Phys. Rev. Lett.*, vol. 89, pp. 240401-1–240401-4, Dec. 2002.

[27] V. D'Ambrosio *et al.*, "Photonic polarization gears for ultra-sensitive angular measurements," *Nature Commun.*, vol. 4, pp. 2432-1–2432-8, Sep. 2013.

[28] T. B. Pittman *et al.*, "Two-photon geometric optics," *Phys. Rev. A*, vol. 53, pp. 2804–2815, Apr. 1996.

[29] A. F. Abouraddy, B. E. A. Saleh, A. V. Sergienko, and M. C. Teich, "Entangled-photon fourier optics," *J. Opt. Soc. Amer. B*, vol. 19, pp. 1174–1184, May 2002.

[30] Y. Q. Qin, C. Zhang, Y. Y. Zhu, X. P. Hu, and G. Zhao, "Wave-front engineering by Huygens–Fresnel principle for nonlinear optical interactions in domain engineered structures," *Phys. Rev. Lett.*, vol. 100, pp. 063902-1–063902-4, Feb. 2008.

[31] Z. Y. J Ou, *Multi-Photon Quantum Interference*. New York, NY, USA: Springer, 2007.

[32] A. Bahabad and A. Arie, "Generation of optical vortex beams by nonlinear wave mixing," *Opt. Exp.*, vol. 15, pp. 17619–17624, Dec. 2007.

[33] G. Poberaj *et al.*, "Ion-sliced lithium niobate thin films for active photonic devices," *Opt. Mater.*, vol. 31, pp. 1054–1058, May 2009.

[34] H. Y. Leng *et al.*, "On-chip steering of entangled photons in nonlinear photonic crystals," *Nature Commun.*, vol. 2, pp. 429-1–429-5, Aug. 2011.

[35] M. W. Mitchell, J. S. Lundeen, and A. M. Steinberg, "Super-resolving phase measurements with a multiphoton entangled state," *Nature*, vol. 429, pp. 161–164, May 2004.

[36] A. N. Boto *et al.*, "Quantum interferometric optical lithography: Exploiting entanglement to beat the diffraction limit," *Phys. Rev. Lett.*, vol. 85, pp. 2733–2736, Sep. 2000.

[37] Z. Y. Ou, X. Y. Zou, L. J. Wang, and L. Mandel, "Experiment on nonclassical fourth-order interference," *Phys. Rev. A*, vol. 42, pp. 2957–2965, Sep. 1990.

[38] J. G. Rarity *et al.*, "Two-photon interference in a Mach–Zehnder interferometer," *Phys. Rev. Lett.*, vol. 65, pp. 1348–1351, Sep. 1990.

[39] E. Megidish *et al.*, "Compact 2D nonlinear photonic crystal source of beamlike path entangled photons," *Opt. Exp.*, vol. 21, pp. 6689–6696, Mar. 2013.

[40] H. Jin *et al.*, "Compact engineering of path-entangled sources from a monolithic quadratic nonlinear photonic crystal," *Phys. Rev. Lett.*, vol. 111, pp. 023603-1–023603-5, Jul. 2013.

[41] H. Kim, H. S. Park, and S. K. Choi, "Three-photon N00N states generated by photon subtraction from double photon pairs," *Opt. Exp.*, vol. 17, pp. 19720–19726, Oct. 2009.

[42] B. Y. Wei *et al.*, "Generating switchable and reconfigurable optical vortices via photopatterning of liquid crystals," *Adv. Mater.*, vol. 26, pp. 1590–1595, Mar. 2014.

[43] S. Sharabi, N. Voloch-Bloch, I. Juwiler, and A. Arie, "Dislocation parity effects in crystals with quadratic nonlinear response," *Phys. Rev. Lett.*, vol. 112, pp. 053901-1–053901-5, Feb. 2014.

[44] G. H. Shao Z. J. Wu, J. H. Chen, F. Xu, and Y. Q Lu, "Nonlinear frequency conversion of fields with orbital angular momentum using quasi-phase-matching," *Phys. Rev. A*, vol. 88, pp. 063827-1–063827-7, Dec. 2013.

[45] M. J. Padgett and J. P. Lesso, "Dove prisms and polarized light," *J. Mod. Opt.*, vol. 46, pp. 175–179, Feb. 1999.

[46] I. Moreno, G. Paez, and M. Strojnik, "Polarization transforming properties of Dove prisms," *Opt. Commun.*, vol. 220, pp. 257–268, May 2003.

[47] L. Marrucci, C. Manzo, and D. Paparo, "Optical spin-to-orbital angular momentum conversion in inhomogeneous anisotropic media," *Phys. Rev. Lett.*, vol. 96, pp. 163905-1–163905-4, Apr. 2006.

[48] M. P. J. Lavery, F. C. Speirits, S. M. Barnett, and M. J. Padgett, "Detection of a spinning object using light's orbital angular momentum," *Science*, vol. 341, pp. 537–540, Aug. 2013.

[49] F. Tamburini, B. Thidé, G. Molina-Terriza, and G. Anzolin, "Twisting of light around rotating black holes," *Nature Phys.*, vol. 7, pp. 195–197, Mar. 2011.

[50] M. Harwit, "Photon orbital angular momentum in astrophysics," *Astrophys. J.*, vol. 597, pp. 1266–1270, Nov. 2003.

[51] K. Shemer *et al.*, "Azimuthal and radial shaping of vortex beams generated in twisted nonlinear photonic crystals," *Opt. Lett.*, vol. 38, pp. 5470–5473, Dec. 2013.

**Yang Ming** is currently working toward the Ph.D. degree at the College of Engineering and Applied Sciences, Nanjing University, Nanjing, China, where he is also with the National Laboratory of Solid State Microstructures.

**Jie Tang** is currently working toward the Postgraduate degree with the College of Engineering and Applied Sciences, Nanjing University, Nanjing, China, where he is also with the National Laboratory of Solid State Microstructures.

**Zhao-xian Chen** is currently working toward the Postgraduate degree with the College of Engineering and Applied Sciences, Nanjing University, Nanjing, China, where he is also with the National Laboratory of Solid State Microstructures.

**Fei Xu** is currently a Professor with the College of Engineering and Applied Sciences and the National Laboratory of Solid State Microstructures, Nanjing University, Nanjing, China. He has published more than 60 peer-reviewed papers on optoelectronic materials and devices. His current research interests include nanophotonics and fiber optics.

**Li-jian Zhang** is currently a Professor with the College of Engineering and Applied Sciences and the National Laboratory of Solid State Microstructures, Nanjing University, Nanjing, China. He has published about 20 papers in peer-review journals including *Nature Photonics, Nature Materials, and Physical Review Letters*. His research interests include experimental and theoretical aspects of quantum optics, quantum information processing, and interactions between light field and quantum materials.

**Yan-qing Lu** (SM'04) is currently a Professor with the College of Engineering and Applied Sciences and the National Laboratory of Solid State Microstructures, Nanjing University, Nanjing, China.

He holds 40 U.S. and Chinese patents. He has published more than100 peer-reviewed papers on optoelectronic materials and devices. His current research interests include nonlinear optics, fiber optics, and liquid crystal devices.